RSC Advances

PAPER

View Article Online
View Journal | View Issue

Cite this: *RSC Adv.*, 2025, **15**, 18826

Dual modification of nickel nanoclusters for selective detection of glutathione through a competitive displacement mechanism†

Yousef A. Bin Jardan,*[a] Mohamed R. Elmasry,[b] Al-Montaser Bellah H. Ali[c] and Mohamed M. El-Wekil *[c]

Glutathione (GSH) is a vital biomolecule that plays a fundamental role in biological systems, regulating numerous cellular functions. Given its physiological significance, the development of analytical sensors capable of sensitively and selectively detecting GSH is of great importance. In this study, a novel fluorescent probe was designed for the detection of GSH in dietary supplements and human biological fluids. The probe consists of nickel nanoclusters (NiNCs) stabilized by polyethyleneimine (PEI) and dithioerythritol (DTH) (PEI/DTH@NiNCs) as dual-protecting ligands. DTH functions as both a stabilizing and reducing agent, while PEI serves as an additional stabilizer, enhancing the structural integrity and stability of the nanoclusters. The fluorescence emission of PEI/DTH@NiNCs was significantly quenched in the presence of Fe^{3+} ions due to aggregation-induced quenching. However, upon the introduction of GSH, a stronger coordination interaction occurs between GSH and Fe^{3+}, leading to the formation of a more stable chelate complex. This competitive binding disrupts the aggregation process, effectively restoring the fluorescence emission of the probe. Under optimized conditions, the fluorescence response exhibited a linear increase with GSH concentration in the range of 0–250 μM. The limit of detection (LOD), calculated based on the signal-to-noise ratio, was determined to be 7.0 nM. The developed probe was successfully applied for GSH detection in dietary supplements and biological samples, yielding recovery rates ranging from 96.9% to 104.1%, with relative standard deviation (RSD) values between 1.87% and 4.01%.

Received 8th March 2025
Accepted 29th May 2025

DOI: 10.1039/d5ra01681a

rsc.li/rsc-advances

1. Introduction

Glutathione (GSH), a tripeptide, is a pivotal antioxidant present in animals, plants, and microorganisms. As the primary thiol (–SH) compound synthesized within these organisms, it plays an essential role in cellular defense mechanisms.[1,2] Beyond its fundamental biological functions, GSH is associated with therapeutic applications for conditions such as influenza, certain cancers, cystic fibrosis, and diabetes. In the pharmaceutical industry, it is highly regarded for its anti-aging properties, immune-boosting capabilities, and powerful detoxification effects.[3,4] Irregular levels of GSH have been linked to a range of diseases, including cancer, chronic renal failure, Alzheimer's disease, diabetes, liver disorders, heart attacks, and Parkinson's disease.[5] Accurate GSH measurement in biological samples is essential for evaluating and diagnosing these diseases early. Analytical surveys identify HPLC,[6,7] colorimetry,[8,9] and electrochemical[10,11] methods are the most common methods for its determination. However, HPLC technique is time consuming, needing exhaustive pretreatment steps, and complicated instrumentation,[12] while colorimetric methods are of low sensitivity and selectivity.[13] Electrochemical methods distinguished by electrode fouling and low selectivity.[14] In contrast, fluorometric-based sensing methods have several advantages such as short response time, low LOD, selectivity, and simplicity.[15,16] Among fluorescent nanomaterials, metal nanoclusters (MNCs) are distinguished by their ease of synthesis, low toxicity, and remarkable photostability.[17,18] Extensive research has been dedicated to noble metal nanoclusters, particularly gold and silver, as fluorescent probes, owing to their exceptional optical properties.[19,20] Nickel is a preferred choice due to its lower cost and greater abundance compared to gold and silver. Nickel nanoclusters (NiNCs) have garnered significant attention over other metal nanoclusters (*e.g.*, AuNCs, AgNCs) due to their water solubility, biocompatibility, very small size, and good stability.[21,22] The synthesis of MNCs typically relies on proteins or peptides as reductants.

[a]*Department of Pharmaceutics, College of Pharmacy, King Saud University, Riyadh, Saudi Arabia. E-mail: Ybinjardan@ksu.edu.sa*

[b]*School of Chemical Engineering, Sungkyunkwan University (SKKU), Suwon, 16419, Republic of Korea*

[c]*Department of Pharmaceutical Analytical Chemistry, Faculty of Pharmacy, Assiut University, Assiut, 71526, Egypt. E-mail: mohamed.elwakeel@pharm.aun.edu.eg; mohamed.mohamoud@ymail.com*

† Electronic supplementary information (ESI) available. See DOI: https://doi.org/10.1039/d5ra01681a

Compared to biomolecules such as GSH and BSA (bovine serum albumin), polyethyleneimine (PEI) and dithioerythritol (DTH) offer a more stable, cost-effective, and biocompatible alternative that is readily available.[23,24] Double protection of nanoclusters is crucial for their stability, functionality, and application performance. Nanoclusters, especially metal-based ones, are highly reactive due to their high surface energy and small size. Without adequate protection, they tend to aggregate, oxidize, or degrade, losing their unique properties. Ali *et al.* successfully synthesized double-protected, red-emissive copper nanoclusters (CuNCs) for detecting melamine in dietary supplements, utilizing Hg^{2+} ions as an assisting agent.[24] Similarly, Ren *et al.* developed PEI-functionalized green emitting CuNCs for fluorometric sensing of cobalt and temperature measurement.[25]

Inspired by the aforementioned studies, novel double-protected nickel nanoclusters (NiNCs) were synthesized for the detection of glutathione (GSH). The stabilization was achieved using polyethyleneimine (PEI) and dithiothreitol (DTH), enhancing the nanoclusters' stability and water solubility. In this system, PEI functions as a stabilizer, while DTH serves both as a stabilizer and a reducing agent. The introduction of ferric ions (Fe^{3+}) selectively chelated the thiol (–SH) and amino (NH_2) groups on the NiNCs surface, inducing aggregation and subsequently quenching fluorescence emission through the aggregation-induced quenching (ACQ) phenomenon. Upon the addition of GSH, Fe^{3+} ions were removed from the NiNC surface *via* coordination interactions, restoring the fluorescence emission. The PEI/DTH@NiNCs probe was successfully applied for the quantification of GSH in real samples, demonstrating satisfactory recovery percentages.

2. Experimental

2.1. Chemicals and instruments

Glutathione (GSH, 98.7%), ascorbic acid (97.8%), uric acid (98.1%), dopamine (99.3%), glucose (98.5%), methionine (97.6%), tryptophan (97.3%), lysine (99.5%), cysteine (98.6%), nickel nitrate hexhydrate ($(Ni(NO_3)_2 \cdot 6H_2O)$), 2-[4-(2-hydroxyethyl)piperazin-1-yl]ethanesulfonic acid (HEPES), dithioerythritol (DTH), polyethyleneimine (PEI), ferric chloride hexahydrate ($FeCl_3 \cdot 6H_2O$), NaOH, and HCl were purchased from Sigma Alrich.

Fluorescence intensity was analyzed using a Shimadzu RF-5301 PC, while UV-Vis absorbance measurements were performed with a Shimadzu 1601 PC (both from Tokyo, Japan). X-ray photoelectron spectroscopy (XPS) spectra were acquired using a Thermo EscalAB 250Xi (Thermo Fisher Scientific, USA), whereas Fourier transform infrared (FT-IR) spectra were recorded with a Nicolet™ iSTM10 (Varian, USA). Dynamic light scattering (DLS) and zeta potential assessments were conducted with a ZEN 3600 Nano ZS (Malvern, UK). The morphological characterization of PEI/DTH@NiNCs was carried out using a JEOL JEM-100CX II transmission electron microscope (USA), while their crystallographic properties were examined *via* X-ray diffraction (XRD) analysis using a Philips-FEI PW 1710 spectrometer (Netherlands).

2.2. Preparation of PEI/DTH@NiNCs

The optimized synthesis conditions for PEI/DTH@NiNCs were as follows: 0.87 g of PEI and 1.17 g of DTH were dissolved in 30 mL of deionized water (DIW) under sonication for 10 minutes to ensure complete dispersion. The pH of the resulting solution was then adjusted to 10.0 by the dropwise addition of NaOH. Subsequently, 3.2 mL of 80.0 mM $Ni(NO_3)_2 \cdot 6H_2O$ was added to the solution, and the mixture was heated to 90 °C for five hours to facilitate the formation of NiNCs. After heating, the solution was allowed to cool to room temperature. The resulting colloidal suspension was then filtered and subjected to dialysis (MWCO = 2000 Da) for 48 hours, with the dialysis water replaced every 8 hours to ensure the complete removal of unreacted species and byproducts. Finally, the purified suspension was freeze-dried and lyophilized, yielding a fine powder of PEI/DTH@NiNCs suitable for further characterization and application.

2.3. Detection procedures

A volume of 250 μL of PEI/DTH@NiNCs (15 mg mL^{-1}) was mixed with 300 μL of HEPES buffer (pH 7.0). Subsequently, 300 μL of 25.0 mM Fe^{3+} was added to the prepared solution and the reaction was initiated at room temperature for 6 minutes. Following this, 150 μL of GSH at varying concentrations was introduced, and the reaction mixture was incubated at room temperature for an additional 3 minutes. After excitation at 335 nm, the fluorescence spectra were recorded at 465 nm.

2.4. Real sample analysis

Ten dietary supplement containing capsules (500 mg each) were weighed, and the average weight of a single capsule was dispersed in 30 mL of DIW, then diluted to 100 mL with DIW and sonicated for 20 minutes. The resulting dispersion was filtered, and the filtrate was analyzed before and after the addition of GSH using the standard addition method.

Human biological samples were analyzed using the proposed method after a 20× dilution with HEPES buffer (pH 7.0). GSH levels were quantified both before and after spiking. The study adhered to Egyptian regulations, received approval from the Ethics Committee of Assiut University, and obtained informed consent from all participants.

3. Results and discussions

3.1. Characterization

The as-fabricated PEI/DTH@NiNCs probe was first characterized using TEM to examine its morphological properties (Fig. 1A). The nanoparticles exhibited a well-dispersed pattern with a spherical shape. The particle sizes of PEI/DTH@NiNCs ranged from 1.2 to 2.7 nm, with an average diameter of 2.2 nm. The inset of the TEM image shows a high-resolution TEM (HRTEM) image, revealing a lattice fringe spacing of 0.22 nm, which aligns well with previously reported literature.[26] The functional groups on the surfaces of DTH, PEI, and PEI/DTH@NiNCs were analyzed using FTIR (Fig. 1B). The FTIR spectrum of DTH (Fig. 1B(a)) exhibits absorption bands at 3236,

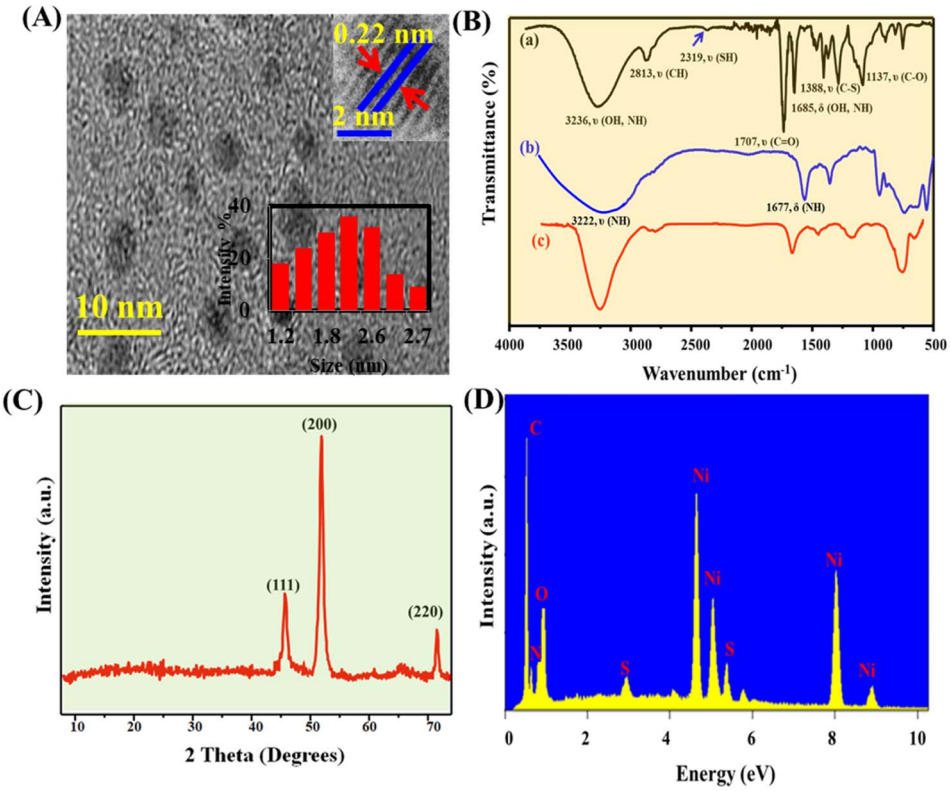

Fig. 1 (A) TEM image (inset is particle distribution and HRTEM); (B) FTIR spectra of DTH, PEI, and PEI/DTH@NiNCs; (C) XRD pattern of PEI/DTH@NiNCs; (D) EDX of PEI/DTH@NiNCs.

2813, 2319, 1707, 1685, 1388, and 1137 cm^{-1}, corresponding to ν(OH, NH), ν(CH), ν(SH), ν(C=O), δ(OH, NH), ν(C–S), and ν(C–O), respectively. The FTIR spectrum of PEI (Fig. 1B(b)) shows an absorption bands at 3222 cm^{-1} and 1677 cm^{-1}, attributed to ν(NH) and δ(NH), respectively. After the modification of NiNCs with DTH and PEI, the main absorption bands of DTH and PEI were retained, except for the disappearance of the SH group in DTH, indicating the successful formation of PEI/DTH@NiNCs (Fig. 1B(c)). Moreover, the crystal structure of the PEI/DTH@NiNCs was investigated using XRD (Fig. 1C). The diffraction peaks at 46.8°, 52.8°, and 73.1° suggest a face-centered cubic (FCC) structure of metallic nickel, corresponding to the (111), (200), and (220) planes, confirming the crystalline nature of the nanoclusters (JCPDS Card No. 04-0850). The EDX pattern of PEI/DTH@NiNCs shown in Fig. 1D suggests the existence of five sharp peaks corresponding to C, N, O, S, and Ni. The presence of sharp peaks suggests that the elements are well-distributed and possibly indicate a strong interaction between the organic matrix (PEI/DTH) and NiNCs. Fig. S1† presents the EDX mapping of the elements in PEI/DTH@NiNCs, revealing their heterogeneous distribution. Fig. S2A† presents the full XPS spectrum of PEI/DTH@NiNCs, highlighting prominent peaks corresponding to C 1s, N 1s, O 1s, S 2p, and Ni 2p. The detailed C 1s spectrum reveals three main peaks at 287.4 eV, 289.5 eV, and 290.8 eV, indicating the presence of C–C/C=C, C–N, and C=O, respectively (Fig. S2B†). The deconvoluted XPS spectrum of N 1s reveals the presence of pyridine N, quaternary N, and pyrrole N, with binding energies at 402.1 eV, 403.3 eV, and 403.9 eV, respectively (Fig. S2C†). Fig. S2D† presents the detailed XPS spectrum of O 1s, featuring sharp peaks corresponding to C–O, C–OH, and C=O, with binding energies of 532.2 eV, 533.7 eV, and 534.8 eV, respectively. The deconvoluted XPS spectrum of S 2p (Fig. S2E†) exhibits prominent peaks corresponding to C–S/C=S and C–Sox, with binding energies of 162.3 eV and 170.8 eV, respectively. Two distinct peaks, as depicted in Fig. S2F,† were observed in the XPS spectrum of Ni 2p at binding energies of 861.3 eV and 869.7 eV, corresponding to Ni $2p_{3/2}$ and Ni $2p_{1/2}$, respectively.[22]

The fluorescence characteristics of PEI/DTH@NiNCs are presented in Fig. 2. The fluorescent probe exhibited an emission peak at 465 nm upon excitation at 335 nm (Fig. 2A). Additionally, excitation wavelengths were varied between 280 nm and 370 nm (Fig. 2B), revealing that maximum emission occurred at 335 nm, which was subsequently used for GSH determination. The excitation-independent emission behavior indicates that the nanoclusters possess a homogeneous surface composition, with uniformly distributed functional groups, resulting in consistent electronic transitions across all particles.[23] The fluorescence quantum yield was determined using quinine sulfate as a reference and calculated to be 19.78%.[24,25] The stability of the fluorescent interface was evaluated under different conditions (Fig. S3†), demonstrating that PEI/DTH@NiNCs exhibit excellent stability. These findings confirm their potential applicability in biosensing.

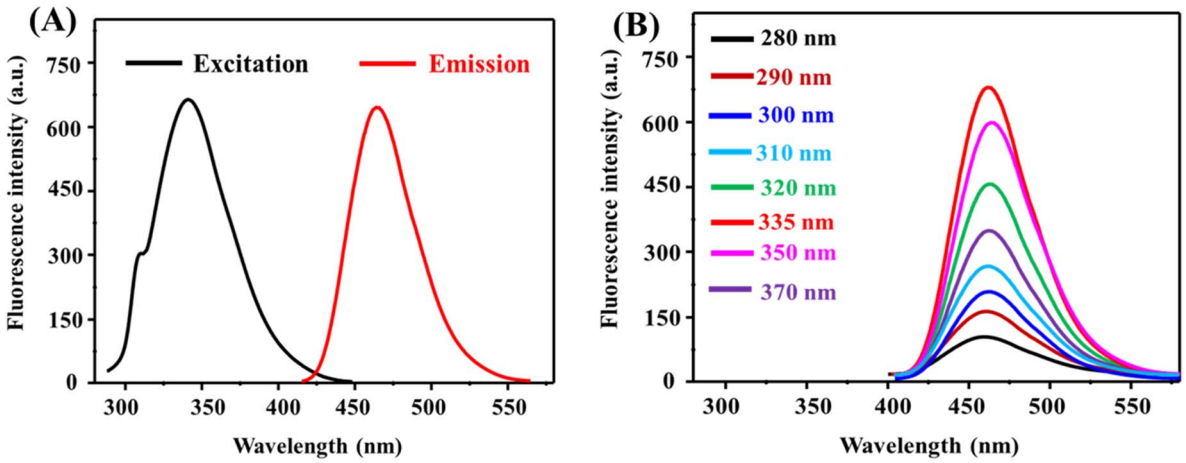

Fig. 2 (A) Excitation/emission spectra of PEI/DTH@NiNCs; (B) emission-independent excitation behavior of PEI/DTH@NiNCs.

3.2. Optimization of variables

To improve the detection sensitivity of the fluorometric method, key variables influencing both the synthesis of the probe and its interaction with GSH were systematically optimized. Notably, NiNCs modified individually with either PEI or DTH exhibited low fluorescence intensity. However, when NiNCs were co-modified with PEI as a stabilizer and DTH as both a stabilizer and a reducing agent, a significant enhancement in fluorescence intensity was observed. Based on these findings, PEI/DTH-functionalized NiNCs were selected as a highly fluorescent probe for the sensitive and selective determination of GSH. To validate this approach, a series of spectroscopic analyses and zeta potential measurements were conducted. As illustrated in Fig. S4A,† the UV-Vis spectra of different ligands and ligand-modified Ni revealed that only the PEI/DTH@NiNCs exhibited a notably strong absorption at 258 nm and 316 nm, which are attributed to ligand–metal charge transfer and interband transitions in NiNCs. These results underscore the crucial role of dual functionalization in enhancing the probe's fluorescence properties, thereby improving its analytical performance for GSH detection. Furthermore, the fluorescence emission spectra of various ligands and ligand-modified NiNCs are presented in Fig. S4B.† The results clearly demonstrate that PEI/DTH@NiNCs exhibit the highest fluorescence emission among all tested ligands/probes. This superior fluorescence performance further confirms the synergistic effect of PEI and DTH in enhancing the optical properties of NiNCs, making them a highly effective probe for GSH detection. The zeta potential values of various ligands and ligand-modified NiNCs were measured to assess their surface charge characteristics (Fig. S4C†). The results indicate that the zeta potential values for PEI, DTH, and PEI/DTH were 6.78 mV, −24.45 mV, and −12.78 mV, respectively. However, upon the introduction of nickel ions, these values shifted to −7.58 mV, −15.78 mV, and −18.56 mV for PEI/Ni, DTH/NiNCs, and PEI/DTH@NiNCs, respectively. This significant decrease in zeta potential for PEI/DTH@NiNCs upon Ni^{2+} coordination suggests enhanced electrostatic interactions and improved colloidal stability of the modified NiNCs. The pronounced change in surface charge further supports the successful functionalization of NiNCs and their potential for effective interaction with GSH in fluorometric applications. The high negative charge of PEI/DTH@NiNCs is attributed to the strong reducing power of DTH, which contribute to the formation of NiNCs with a negatively charged surface. While DTH serves as both a stabilizer and a reducing agent, PEI primarily functions as an effective stabilizer, enhancing the long-term stability of the probe. PEI stabilizes the NiNCs through steric hindrance and the formation of N–Ni covalent bonds, which prevent aggregation and improve colloidal stability. Furthermore, the lone pair of electrons on the PEI molecules facilitates additional interactions with nickel ions *via* Lewis acid–Lewis base chemical interactions, further reinforcing the structural integrity of the nanoclusters.[27,28] The reaction variables were optimized, including the amounts of PEI and DTH, reaction temperature, and reaction time (Fig. S5†). The optimal conditions were determined to be 0.87 g of PEI, 1.17 g of DTH, a reaction temperature of 90 °C, and a reaction time of five hours.

The factors influencing the chemical reaction between GSH and the probe (PEI/DTH@NiNCs/Fe^{3+}) were evaluated (Fig. 3). Fig. 3A illustrates the effect of PEI/DTH@NiNCs volume, ranging from 50 to 400 μL. The results indicate that maximum fluorescence was achieved at 250 μL. Beyond this volume, increasing PEI/DTH@NiNCs did not significantly enhance fluorescence emission, suggesting that 250 μL is the optimal volume for subsequent determinations. Fig. 3B examines the impact of different metal ions on the quenching of PEI/DTH@NiNCs fluorescence. Among the tested metals, Fe^{3+} exhibited the most pronounced fluorescence quenching effect, indicating its strong interaction with the probe. Furthermore, the influence of Fe^{3+} concentration on fluorescence response was analyzed (Fig. 3C and D). The results showed that maximum quenching was achieved at 25.0 μM Fe^{3+}. The effect of pH on the fluorescence response was investigated over a range of 5.0 to 9.0, as illustrated in Fig. 3E. The results demonstrate that the optimal fluorescence response occurs at

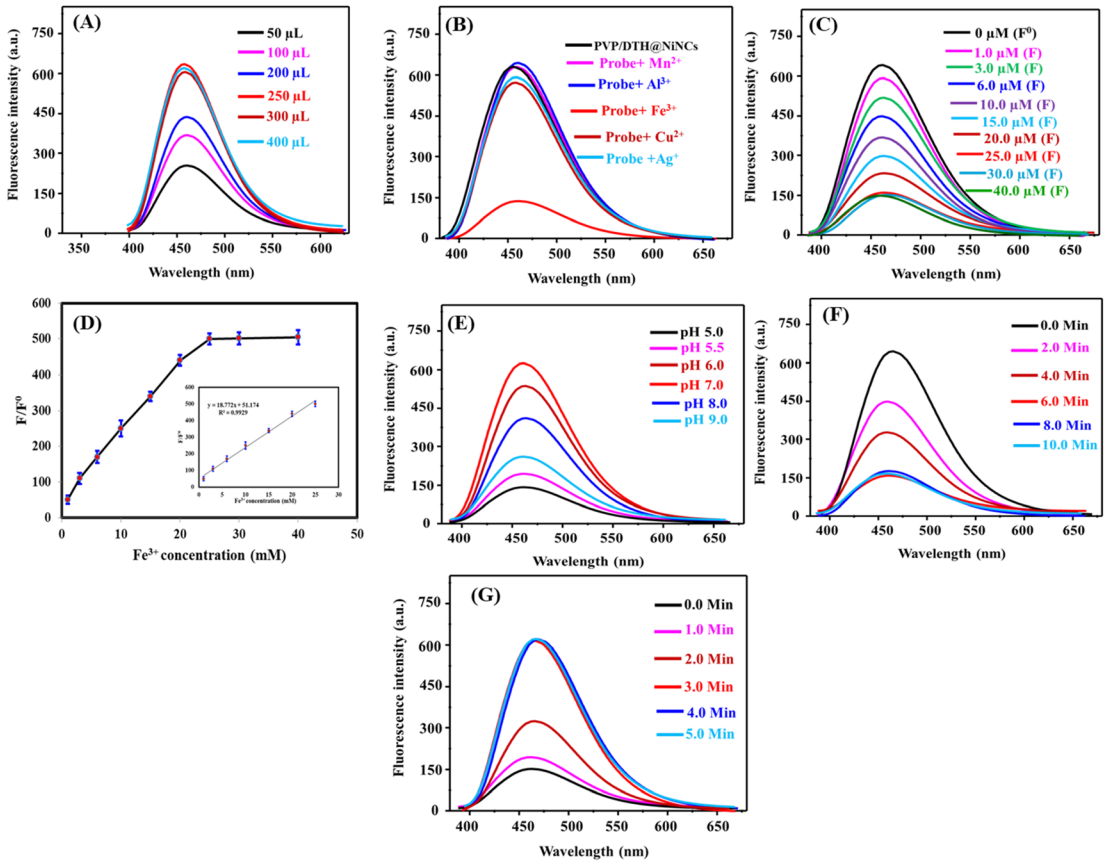

Fig. 3 Influence of the detection parameters: (A) volume of PEI/DTH@NiNCs, (B) different metal ions (25.0 μM), (C) different Fe^{3+} concentration (0–40 μM), (D) calibration plot between F/F^0 and concentration of Fe^{3+} ion, (E) pH value, (F) reaction time between PEI/DTH@NiNCs and 25.0 μM Fe^{3+} ion, (G) reaction time between PEI/DTH@NiNCs/Fe^{3+} and GSH.

pH 7.0. Under acidic conditions, Fe^{3+} exists in a less reactive form and the –SH group of GSH is protonated, significantly reducing its reactivity. In contrast, under alkaline conditions, Fe^{3+} tends to precipitate as $Fe(OH)_3$, limiting its solubility and preventing effective interactions with both the fluorescent probe and GSH. These findings highlight the critical role of pH in modulating the reactivity of Fe^{3+} and the overall sensing mechanism. The effect of quenching time between PEI/DTH@NiNCs and Fe^{3+} ion was demonstrated in Fig. 3F. It was found that the maximum quenching of PEI/DTH@NiNCs by Fe^{3+} ions was achieved after six minutes, while the optimal reaction time for recovering PEI/DTH@NiNCs after the addition of GSH was three minutes, as depicted in Fig. 3G. The response time is calculated by measuring how fast the sensor's signal changes after adding analyte. The signal was tracked until it stops changing much, and the time it takes to reach that point is recorded as the response time.

3.3. Mechanism

To illustrate the detection mechanism of the proposed strategy, a series of spectroscopic analyses, size measurements, morphological assessments, and zeta potential recordings were conducted (Fig. S6†). TEM images (Figs. S6A and B†) display PEI/DTH@NiNCs after the addition of Fe^{3+} and GSH, respectively. A significant increase in particle size was observed upon Fe^{3+} introduction, indicating aggregation. Conversely, the addition of GSH reduced the particle size, suggesting the removal of Fe^{3+} from the probe's surface. Dynamic light scattering (DLS) measurements further confirmed these findings. The particle diameter of PEI/DTH@NiNCs/Fe^{3+} was recorded at 448.65 nm, which decreased to 82.89 nm after GSH addition, demonstrating the disassembly of Fe^{3+}-induced aggregates (Fig. S6C†). To investigate the quenching mechanism between PEI/DTH@NiNCs and Fe^{3+}, spectroscopic analyses were performed. Fig. S6D† presents the UV/Vis spectrum of Fe^{3+} ions alongside the excitation spectrum of PEI/DTH@NiNCs. Partial overlap between the two spectra was observed, confirming the presence of an inner-filter effect.[29,30] Furthermore, fluorescence lifetime measurements were conducted for PEI/DTH@NiNCs, PEI/DTH@NiNCs/Fe^{3+}, and PEI/DTH@NiNCs/Fe^{3+}/GSH, yielding values of 4.84 ns, 4.76 ns, and 4.82 ns, respectively (Fig. S6E†). These minimal variations suggest the occurrence of static quenching, which supports a non-collisional, complexation-based interaction.[31] Zeta potential measurements were conducted, as shown in Fig. S6F.† The recorded values for PEI/DTH@NiNCs, PEI/DTH@NiNCs/Fe^{3+}, and PEI/DTH@NiNCs/Fe^{3+}/GSH were −16.78 mV, −5.98 mV, and −12.56 mV, respectively. This shift indicates that GSH altered

the surface chemistry by removing Fe^{3+} ions through a direct interaction. Together, these findings point to coordination interaction as the dominant mechanism. GSH, which contains both thiol and amino groups, has a strong binding affinity toward Fe^{3+}, forming a stable chelate that removes Fe^{3+} from the nanocluster surface, thereby restoring fluorescence.[32] The collective evidence—structural (TEM, DLS), spectral (UV/Vis), electrokinetic (zeta potential), and photophysical (fluorescence lifetime)—strongly supports that: (i) Fe^{3+} binds to the surface of PEI/DTH@NiNCs *via* coordination with amino and thiol groups, inducing aggregation and fluorescence quenching. (ii) GSH then competes and replaces these interactions through its stronger bidentate coordination with Fe^{3+} (*via* –SH and $–NH_2$ groups), displacing Fe^{3+}, disaggregating the clusters, and restoring fluorescence. Thus, coordination interaction is the primary mechanism, rather than redox or simple electrostatic displacement.

3.4. Sensitivity of PEI/DTH@NiNCs Fe^{3+} system towards GSH detection

After optimizing the experimental parameters, the proposed system was employed to measure the fluorescence response of GSH at varying concentrations. Fig. 4A illustrates the emission spectra of the PEI/DTH@NiNCs/Fe^{3+} system upon the successive addition of GSH in the concentration range of 0–250 μM. Within this linear range, the fluorescence recovery ratio exhibited a proportional increase with rising GSH concentrations. The relationship between fluorescence intensity and GSH concentration was characterized by the following linear regression equation: $[F/F^0] = 1.229 + 0.011C_{GSH}$ where F and F^0 represent the fluorescence emission intensities of the probe after and before GSH addition, respectively (Fig. 4B). The detection limit was determined using a signal-to-noise ratio of 3 : 1, yielding a sensitivity of 7.0 nM. To highlight the significance of the proposed system, its analytical performance was benchmarked against other colorimetric and fluorometric sensors. The results demonstrated that this sensor offers distinct advantages, including ultra-low detection limits, rapid response times, a broad linear range, and cost-effectiveness (Table 1). These attributes make it a promising tool for highly sensitive GSH detection in various applications.

3.5. Reproducibility and selectivity/anti-interference studies

Reproducibility is a critical parameter in assessing the reliability of the proposed sensor for detecting the target analyte. To evaluate this, eight independently prepared PEI/DTH@NiNCs/Fe^{3+} sensors, fabricated under identical conditions, were tested for the detection of 10.0 μM GSH. The results

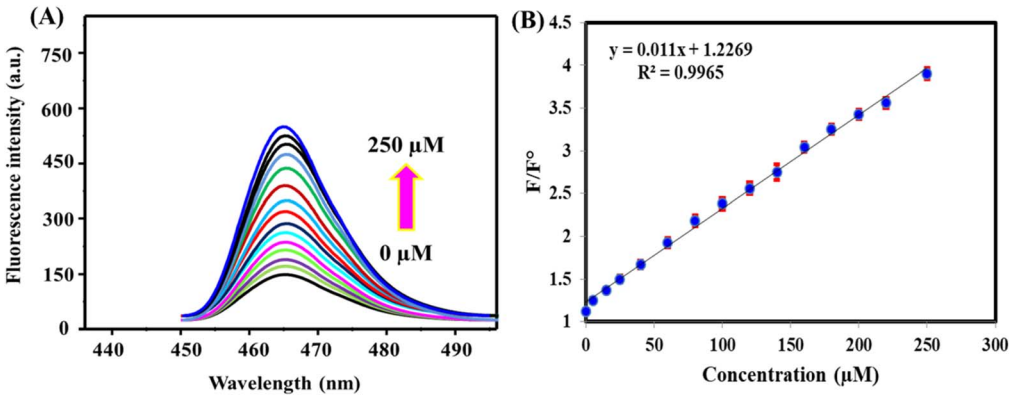

Fig. 4 (A) The FL signal spectra of PEI/DTH@NiNCs Fe^{3+} system after addition of GSH in the range of 0 to 250 μM. (B) Calibration plot between F/F^0 and concentration of GSH.

Table 1 Comparison of PEI/DTH@NiNCs/Fe^{3+} and other sensors for determination of GSH

Method	Sensor/system	Linear range (μM)	LOD (μM)	Response time (min)	Reference
Colorimetry	Mn-doped CDs/AgNPs	0–300	0.53	3	33
	Fe_3O_4@polypyrrole	0.5–80	0.15	30	34
	FeOCl NS	3–33	2.23	30	35
	A g-CDs	1–60	0.38	20	36
	CoOOH NS	33–1300	13.7	10	37
Fluorescence	*N*,*S*-CQDs	0.1–200	0.07	3	38
	PEI@CDs	0–50	0.062	3	39
	Eu-doped CDs	0–50	0.03	2	40
	MnO_2/polydopamine	0–350	1.5	5	41
	Ag/Au NCs/Fe^{3+}	0.03–95	0.009	5	42
	PEI/DTH@NiNCs/Fe^{3+}	0–250	0.007	3	This work

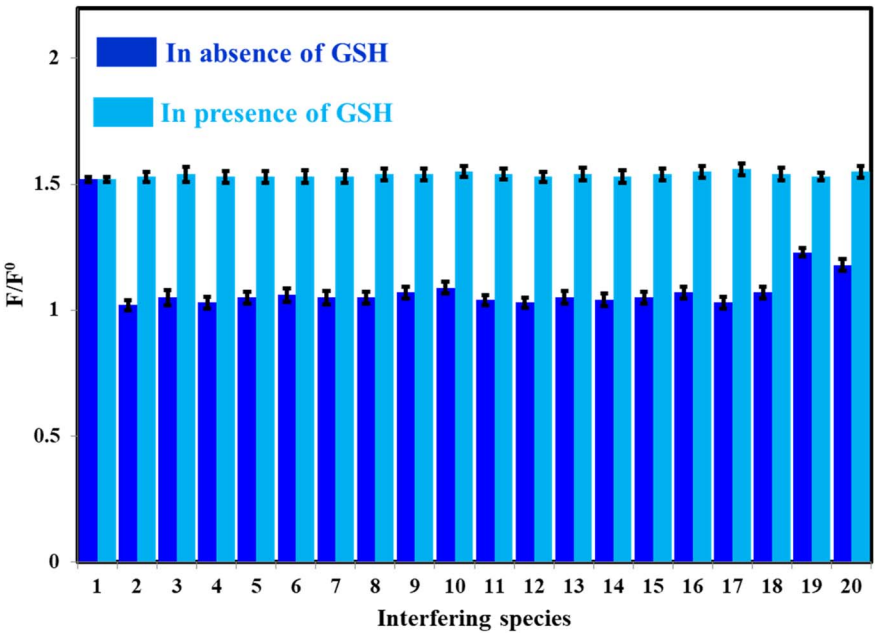

Fig. 5 Selectivity and anti-interference evaluation of PEI/DTH@NiNCs/Fe^{3+} in the presence of 25.0 μM GSH (1) and a 30-fold concentration of various potential interfering species. Interfering ions are represented as follows: (2–12) correspond to K^+, Na^+, Mg^{2+}, Ca^{2+}, Ba^{2+}, Li^+, HCO_3^-, Cl^-, CO_3^{2-}, SO_4^{2-}, and PO_4^{3-}, while (13–20) represent small biomolecules, including lysine, uric acid, dopamine, glucose, tryptophan, methionine, cysteine, and ascorbic acid.

demonstrated that the relative standard deviation (RSD) did not exceed 3.08%, indicating the high precision and accuracy of the proposed sensor for GSH quantification.

Selectivity is a critical parameter that determines the practical applicability of the proposed method. To evaluate this, the as-fabricated sensing system was employed to measure 25.0 μM GSH in the presence of a 30-fold concentration of potential interfering species, both separately (to assess selectivity) and in combination (to evaluate anti-interference effects). The tested interfering species included various ions (K^+, Na^+, Mg^{2+}, Ca^{2+}, Ba^{2+}, Li^+, HCO_3^-, Cl^-, CO_3^{2-}, SO_4^{2-}, PO_4^{3-}) and small biomolecules (lysine, uric acid, dopamine, glucose, tryptophan, methionine, cysteine, and ascorbic acid). These species are abundant in biological fluids and may potentially interfere with the sensing mechanism. Testing against them ensures that the probe's response is specific to Fe^{3+}, confirming its reliability and selectivity in complex biological matrices. The results demonstrated that GSH induced a significant enhancement in fluorescence response due to the formation of a stable chelate complex between GSH and Fe^{3+} ions (Fig. 5). Notably, cysteine

Table 2 Applications of PEI/DTH@NiNCs/Fe^{3+} for detecting GSH in real samples ($n = 4$)

		PEI/DTH@NiNCs/Fe^{3+}			Standard HPLC method[43]		
Sample	Amount added (μM)	Found (μM)	Recovery (%)	RSD (%)	Found (μM)	Recovery (%)	RSD (%)
Dietary supplement	0.0	6.98	—	3.08	7.34	—	3.64
	2.0	9.35	104.1	2.87	9.76	104.5	4.23
	5.0	11.78	98.3	3.65	12.67	102.7	3.87
	10.0	16.58	97.6	1.87	17.09	98.6	4.67
Urine	0.0	7.26	—	2.65	6.98	—	3.76
	2.0	9.47	102.3	3.29	9.34	104.0	3.65
	5.0	12.53	102.2	1.85	11.75	98.0	4.39
	10.0	17.14	99.3	3.65	17.42	102.6	4.87
Serum	0.0	10.25	—	2.78	10.76	—	3.52
	2.0	12.56	102.5	3.08	13.08	102.5	3.87
	5.0	15.76	103.3	3.67	16.00	101.5	2.76
	10.0	19.97	98.6	2.24	21.13	101.7	4.19
Saliva	0.0	5.56	—	3.27	5.78	—	2.87
	2.0	7.35	97.2	2.50	8.08	103.9	3.65
	5.0	10.24	96.9	3.78	11.26	104.5	2.54
	10.0	15.98	102.7	4.01	15.02	95.2	4.75

and ascorbic acid exhibited slight interference by moderately increasing the fluorescence signal. This interference may be attributed to the ability of cysteine to chelate Fe^{3+} ions, albeit with a lower binding affinity compared to GSH. Additionally, ascorbic acid was found to reduce Fe^{3+} ions, thereby diminishing their influence on the aggregation of the fluorescent probe. These interfering compounds, ascorbic acid and cysteine, are typically present at significantly lower concentrations than GSH,[42] minimizing their impact on the sensor's performance.

3.6. Real samples analysis

The as-prepared sensing system was applied for GSH detection across various sample matrices with different GSH concentrations. The fluorometric method was employed both before and after spiking with known amounts of GSH. The recovery rates for all samples ranged from 96.9% to 104.1%, with relative standard deviation (RSD) values between 1.87% and 4.01%. Furthermore, the performance of the proposed method was validated by comparing the results with those obtained using a reported HPLC/UV method.[43] As presented in Table 2, the findings confirm the high accuracy of the fluorometric approach, highlighting its potential for reliable GSH quantification in complex matrices.

4. Conclusion(s)

In this study, a novel fluorometric system was developed for the selective and sensitive detection of GSH. The sensing probe consists of nickel nanoclusters (NiNCs) functionalized with polyethyleneimine (PEI) and dithioerythritol (DTH), which enhance stability and facilitate the reduction of Ni^{2+} ions during nanocluster formation. The resulting PEI/DTH@NiNCs probe exhibit strong fluorescence intensity and excellent stability under varying conditions. Upon the introduction of Fe^{3+}, strong chelation occurs between Fe^{3+} and the amino and thiol groups on the probe's surface, inducing aggregation-mediated fluorescence quenching. However, in the presence of GSH, fluorescence recovery is observed due to the preferential coordination of GSH with Fe^{3+}, leading to the formation of a stable chelate complex. Under optimized conditions, the probe demonstrated a low LOD, high selectivity, and a rapid response time for GSH quantification. Furthermore, the fluorescent sensor was successfully applied for GSH detection in urine, serum, saliva, and dietary supplements, yielding satisfactory results, confirming its potential for real-world analytical applications. Nickel's known cytotoxicity and potential to elicit allergic or inflammatory responses may restrict its use in biomedical applications, particularly for *in vivo* diagnostics or therapeutic platforms. Strategies to mitigate this include encapsulation, doping, or substituting with more biocompatible metals.

Data availability

Data will be available upon request from the corresponding authors.

Conflicts of interest

The authors state that there are no conflicts of interest, financial or personal, that could have affected the integrity of this work.

Acknowledgements

The authors thank the Ongoing Research Funding Program (ORF-2025-457), King Saud University, Riyadh, Saudi Arabia for supporting this research work.

References

1 K. Alhazzani, A. Z. Alanazi, A. M. Mostafa, J. Barker, M. M. El-Wekil and A. B. H. Ali, A dual emissive silver-riboflavin complex and nitrogen-doped carbon dot nanoprobe for ratiometric detection of glutathione, *Microchem. J.*, 2024, **199**, 109996.
2 A. M. Mahmoud, B. A. Alyami, M. H. Mahnashi, F. M. Alshareef, Y. S. Alqahtan and M. M. El-Wekil, Facile fabrication of a superior electrochemical sensor with antifouling properties for sensitive and selective determination of glutathione, *Microchem. J.*, 2023, **187**, 108419.
3 D. M. Minich and B. I. Brown, A review of dietary (phyto) nutrients for glutathione support, *Nutrients*, 2019, **11**, 2073.
4 A. Habib, M. M. Mabrouk, M. Fekry and F. R. Mansour, Glycerol as a new mobile phase modifier for green liquid chromatographic determination of ascorbic acid and glutathione in pharmaceutical tablets, *J. Pharm. Biomed. Anal.*, 2022, **219**, 114870.
5 M. Hanko, L. Svorc, A. Plankova and P. Mikus, Overview and recent advances in electrochemical sensing of glutathione – a review, *Anal. Chim. Acta*, 2019, **1062**, 1–27.
6 O. Mompó-Roselló, M. Vergara-Barberán, E. F. Simó-Alfonso and J. M. Herrero-Martínez, In syringe hybrid monoliths modified with gold nanoparticles for selective extraction of glutathione in biological fluids prior to its determination by HPLC, *Talanta*, 2020, **209**, 120566.
7 A. Tsiasioti and P. D. Tzanavaras, Determination of glutathione and glutathione disulfide using liquid chromatography: a review on recent applications, *Microchem. J.*, 2023, **193**, 109157.
8 D. Yin, H. Yang, S. Wang, Z. Yang, Q. Liu, X. Zhang and X. Zhang, Ce-doped $ZnCo_2O_4$ nanospheres: synthesis, double enzyme-like performances, catalytic mechanism and fast colorimetric determination for glutathione, *Colloids Surf. A*, 2020, **607**, 125466.
9 S. Sam, S. Swathy and K. G. Kumar, Lysozyme functionalized silver nanoclusters as a dual channel optical sensor for the effective determination of glutathione, *Talanta*, 2024, **277**, 126326.
10 R. Kaimal, A. Dube, A. Al Souwaileh, J. J. Wu and S. Anandan, A copper metal–organic framework-based electrochemical sensor for identification of glutathione in pharmaceutical samples, *Analyst*, 2024, **149**, 947–957.
11 A. M. Mahmoud, M. H. Mahnashi and M. M. El-Wekil, Ratiometric sensing interface for glutathione

determination based on electro-polymerized copper-coordinated molecularly imprinted layer supported on silver/porous carbon hybrid, *Anal. Chim. Acta*, 2023, **1272**, 341498.

12 K. Alhazzani, A. Z. Alanazi, A. M. Alaseem, S. A. Al Awadh, S. A. Alanazi, A. A. AlSayyari, M. M. Alanazi and M. M. El-Wekil, A reliable ratiometric fluorescence sensing of heparin and its antidote based on cationic carbon quantum dots and acid red 87, *Microchem. J.*, 2023, **190**, 108666.

13 B. A. Alyami, A. M. Mahmoud, A. O. Alqarni and M. M. El-Wekil, Intrinsic self-calibration electrostatic-controlled ratiometric fluorescence assay of histamine in human serum and canned tuna fish samples, *Microchem. J.*, 2023, **195**, 109388.

14 A. M. Mahmoud, M. H. Mahnashi and M. M. El-Wekil, Ratiometric fluorescence sensing of hazardous ciprofloxacin based on aggregation induced emission enhancement of thiolate-protected gold nanoclusters induced by La^{3+} ion, *Spectrochim. Acta, Part A*, 2024, **304**, 123347.

15 Z. Cheng, L. Gu, Y. Zhao, L. Yang, L. Chen, T. Wang, M. Luo, J. Wei and P. Li, Copper ions assisted fluorescent detection of some dithiocarbamates based on nickel nanocluster with aggregation-induced emission enhancement behavior, *J. Hazard. Mater.*, 2022, **424**, 127555.

16 R. M. K. Mohamed, S. H. Mohamed, A. M. Asran, I. H. Alsohaimi, H. M. A. Hassan, H. Ibrahim and M. M. El-Wekil, Bifunctional ratiometric sensor based on highly fluorescent nitrogen and sulfur biomass-derived carbon nanodots fabricated from manufactured dairy product as a precursor, *Spectrochim. Acta, Part A*, 2023, **293**, 122444.

17 D. Li, Z. Chen and X. Mei, Fluorescence enhancement for noble metal nanoclusters, *Adv. Colloid Interface Sci.*, 2017, **250**, 25–39.

18 X. Kang and M. Zhu, Metal nanoclusters stabilized by selenol ligands, *Small*, 2019, **15**, 1902703.

19 Y. S. Alqahtania, A. M. Mahmouda, A. B. H. Ali and M. M. El-Wekil, Enhanced fluorometric detection of histamine using red emissive amino acid-functionalized bimetallic nanoclusters, *RSC Adv.*, 2024, **14**, 18970–18977.

20 A. Z. Alanazi, K. Alhazzani, H. Ibrahim, A. B. H. Ali, M. Darweesh, R. Y. Shahin and M. M. El-Wekil, Dual emission BSA-capped bimetallic nanoclusters for detection of acrylamide in certain food matrices based on thiol-ene Michael addition click reaction, *Microchem. J.*, 2024, **206**, 111625.

21 Z. H. Cheng, L. Q. Gu, Y. Y. Zhao, L. L. Yang, L. Chen, T. Wang, M. Luo, J. C. Wei and P. Li, Copper ions assisted fluorescent detection of some dithiocarbamates based on nickel nanocluster with aggregation-induced emission enhancement behavior, *J. Hazard. Mater.*, 2022, **424**, 127555.

22 A. M. Mahmoud, A. O. Alqarni, R. Ali and M. M. El-Wekil, Polyvinylpyrrolidone and 4-mercaptobenzoic acid-functionalized nickel nanoclusters for selective and sensitive detection of glutathione assisted by Fe^{3+}, *Anal. Methods*, 2025, **17**, 360–367.

23 Y. Liu, Y. Qing, L. Jing, W. Zou and R. Guo, Platinum-copper bimetallic colloid nanoparticle cluster nanozymes with multiple enzyme-like activities for scavenging reactive oxygen species, *Langmuir*, 2021, **37**, 7364–7372.

24 R. Ali, A. Alattar, A. S. Albalawi, A. Alkhamali, O. A. Hakami, H. H. Alharthi, M. S. Alahmari, A. H. Alharbi, O. M. Aljohani, Y. A. Y. Alzahrani, T. M. Albaqami and M. M. El-Wekil, Developing a switch "OFF-ON" fluorescent probe for detection of melamine based on doubly-protected red emissive copper nanoclusters mediated by Hg^{2+} ions, *Spectrochim. Acta, Part A*, 2025, **326**, 125286.

25 J. Ren, W. Wu, T. Chen, H. Guo, C. Xu, J. Ma, L. Wang, J. Wang and L. Li, Polyethylenimine-protected green-emission copper nanoclusters as highly effective fluorescent and colorimetric nanoprobe for selective cobalt ions and temperature sensing, *Spectrochim. Acta, Part A*, 2024, **304**, 123438.

26 Z. Cheng, T. Wang, M. Luo, S. Wu, S. Hua, Y. Li, Y. Yang, L. Zou, J. Wei and P. Li, A new luminescent nickel nanocluster with solvent and ion induced emission enhancement toward heavy metal analysis, *Biosens. Bioelectron.*, 2024, **264**, 116660.

27 S. Pu, C. Xia, L. Wu and K. Xu, CuNCs modified with dual-ligand to achieve fluorescence visualization detection of Tin (IV), *Microchem. J.*, 2022, **183**, 108086.

28 Y. Zhu, Y. Tang and P. Miao, Block-Polymer-Restricted Sub-nanometer Pt Nanoclusters Nanozyme-Enhanced Immunoassay for Monitoring of Cardiac Troponin I, *Langmuir*, 2024, **40**, 1130–1136.

29 A. M. Mahmoud, M. H. Mahnashi and M. M. El-Wekil, Double protein directed synthesis of chemically etched sulfur doped quantum dots for signal "on-off-on" sensing of glutathione mediated by copper ions, *Anal. Methods*, 2023, **15**, 4296–4303.

30 Y. S. Alqahtani, A. M. Mahmoud, H. Ibrahim and M. M. El-Wekil, Enhanced fluorescent detection of oxaliplatin *via* BSA@copper nanoclusters: a targeted approach for cancer drug monitoring, *Anal. Methods*, 2024, **16**, 3125–3130.

31 M. Tian, Y. Wang and G. Liu, Polyvinylpyrrolidone-stabilized blue-emitting copper nanoclusters as fluorescence probe for selective detection of dopamine, *ChemistrySelect*, 2024, **9**, e202401550.

32 Z. Chen, D. Lu, G. Zhang, J. Yang and C. Dong, Glutathione capped silver nanoclusters-based fluorescent probe for highly sensitive detection of Fe^{3+}, *Sens. Actuators, B*, 2014, **202**, 631–637.

33 S. S. L. Wang, Y. Chen, Y. Ji, S. Zheng, F. Wang and C. Li, Cheap and portable paper chip with terrific oxidase-like activity and SERS enhancement performance for SERS-colorimetric bimodal detection of intracellular glutathione, *Biosens. Bioelectron.*, 2024, **244**, 115817.

34 W. Yang, C. Weng, X. Li, H. He, J. Fei, W. Xu, X. Yan, W. Zhu, H. Zhang and X. Zhou, A sensitive colorimetric sensor based on one-pot preparation of h-Fe_3O_4@ppy with high

peroxidase-like activity for determination of glutathione and H_2O_2, *Sens. Actuators, B*, 2021, **338**, 129844.

35 Z. Mohammadpour, F. M. Jebeli and S. Ghasemzadeh, Peroxidase-mimetic activity of FeOCl nanosheets for the colorimetric determination of glutathione and cysteine, *Microchem. Acta*, 2021, **188**, 239.

36 L. Haiyang, L. Guantong, Z. Nan, Y. Zhanye, J. Xinge, Z. Bing and Y. Tian, Ag-carbon dots with peroxidase-like activity for colorimetric and SERS dual mode detection of glucose and glutathione, *Talanta*, 2024, **273**, 125898.

37 J. Li, L. Jiao, W. Xu, H. Yan, G. Chen, Y. Wu, L. Hu and W. Gu, Cobalt oxyhydroxide nanosheets integrating with metal indicator enable sensitive detection of glutathione, *Sens. Actuators, B*, 2021, **329**, 129247.

38 H. Wang, W. Mu, S. Wang, L. Shi, T. Ma and Y. Lu, Facile synthesis of NS-doped carbon dots as sensitive "ON-OFF-ON" fluorescent sensor for Cu^{2+} and GSH detection, *Spectrochim. Acta, Part A*, 2024, **305**, 123460.

39 X. Li, G. Chen, A. Hu, Y. Xiong, T. Yang, C. Ma, L. Li, H. Gao, C. Zhu, W. Zhang and Z. Cai, Detection of mercury(II) and glutathione using a carbon dots-based "off-on" fluorescent sensor and the construction of a logic gate, *Anal. Bioanal. Chem.*, 2023, **415**, 1397–1409.

40 H. S. Al-mashriqi, P. Sanga, J. Chen, E. Qaed, J. Xiao, X. Li and H. Qiu, Multifunctional Eu-doped carbon dots nanoprobe for highly sensitive and selective determination of glutathione in biological fluid and cell imaging, *Carbon*, 2024, **228**, 119380.

41 X. J. Kong, S. Wu, T. T. Chen, R. Q. Yu and X. Chu, MnO_2-induced synthesis of fluorescent polydopamine nanoparticles for reduced glutathione sensing in human whole blood, *Nanoscale*, 2016, **8**, 15604–15610.

42 Y. S. Alqahtani, A. M. Mahmoud, M. M. Khateeb, R. Ali and M. M. El-Wekil, Near-infrared fluorescent probe for selective and sensitive detection of glutathione based on thioctic acid-functionalized Ag/Au NCs-assisted by ferric ion, *Microchem. J.*, 2024, **201**, 110752.

43 V. Sutariya, D. Wehrung and W. J. Geldenhuys, Development and validation of a novel RP-HPLC method for the analysis of reduced glutathione, *J. Chromatogr. Sci.*, 2012, **50**, 271–276.